Building and Environment, Vol. 22, No. 2, pp. 111–127, 1987.
Printed in Great Britain.

0360-1323/87 $3.00 + 0.00

Calculation of Age and Local Purging Flow Rate in Rooms

LARS DAVIDSON
ERIK OLSSON*

The local purging flow rate and the local age in ventilated rooms are numerically investigated; both quantities are calculated in an isothermally ventilated two-dimensional room, the latter in two buoyantly ventilated three-dimensional rooms as well. When calculating the velocity field in the two-dimensional room a new one-equation turbulence model is used. When compared with experimental data the predictions show a satisfying agreement in most cases. The local purging flow rate has not yet been obtained experimentally; calculation of this quantity thus provides useful information of its nature.

NOMENCLATURE

a_E, a_P, a_W	coefficients defined in Eq. (A2)
B	width of room
b	width of inlet
c	concentration of contaminant
c_0	initial concentration
$C_{1\varepsilon}$, $C_{2\varepsilon}$, C_D, C_μ, C'_μ	constants in turbulence models
D	diffusion in Eq. (A2)
F	convection in Eq. (A2)
G	turbulence generating source term in the k- and ε-equations
G_β	buoyancy source term in the k-equation
g	acceleration due to gravity
H	height of room
h	height of inlet
k	turbulent kinetic energy
L	length of room
L_t	turbulent length scale
$\dot{m}$	mass flow rate
n	normal co-ordinate
p	pressure
Q	total mass (volume) flow rate
r	radial co-ordinate
t	temperature in °C
U, V, W	mean velocity in x-, y- and z-direction, respectively
U_i	mean velocity in x_i-direction
U_P	local purging flow rate
V	volume of the room
x, y, z	cartesian co-ordinates
x_i	cartesian co-ordinate in i-direction

Greek symbols

Γ_ϕ	exchange coefficient of dependent variable
δ	length of side of a quadratic control volume
δ_i	half width of room in i-direction
δx	length of control volume in x-direction
δy	length of control volume in y-direction
ε	dissipation of turbulent kinetic energy
κ	von Karman's constant
λ	slope
μ, μ_{eff}, μ_t	dynamic viscosity (laminar, effective and turbulent, respectively)
ρ	density
σ_c, σ_k, σ_t, σ_ε	turbulent Prandtl number for concentration, turbulent kinetic energy, temperature and dissipation of turbulent kinetic energy, respectively
τ	time
$\bar{\tau}$	average age in a system (room)
τ_n	nominal time constant of system (room) ($\equiv V/Q$)
$\bar{\tau}_P$	local mean age at a point
ϕ	dependent variable; cumulative distribution function for the age
φ	probability density function for the age

Subscripts

e	exit
in	inlet
P	arbitrary point
ref	reference value for the room

* Department of Applied Thermodynamics and Fluid Mechanics, Chalmers University of Technology, S-412 96, Gothenburg, Sweden.

1. INTRODUCTION

A NEW concept of describing ventilation efficiency has recently been introduced by Sandberg and Sjöberg [1] (see also [2]). This concept is based on two new ventilation parameters: the local purging flow rate and the age distribution. The local purging flow rate, U_P, is the local net flow rate at which air is supplied, from the inlet, to an arbitrary point within the room. The local mean age at an arbitrary point is the time τ that has elapsed, on average, since the molecules passing this point entered the room. There is, at the present time, no practical method for measuring the local purging flow rate. The local mean age distribution is, however, relatively easy to obtain experimentally, and has been investigated [3]. Results show that knowledge of the distribution of the local mean age provides useful information on how the air and contaminants spread in ventilated rooms. Such a concept of age is therefore a valuable tool in evaluating the performance of different ventilation schemes.

For these reasons it seemed that it would be valuable to calculate the distribution of the local mean age and

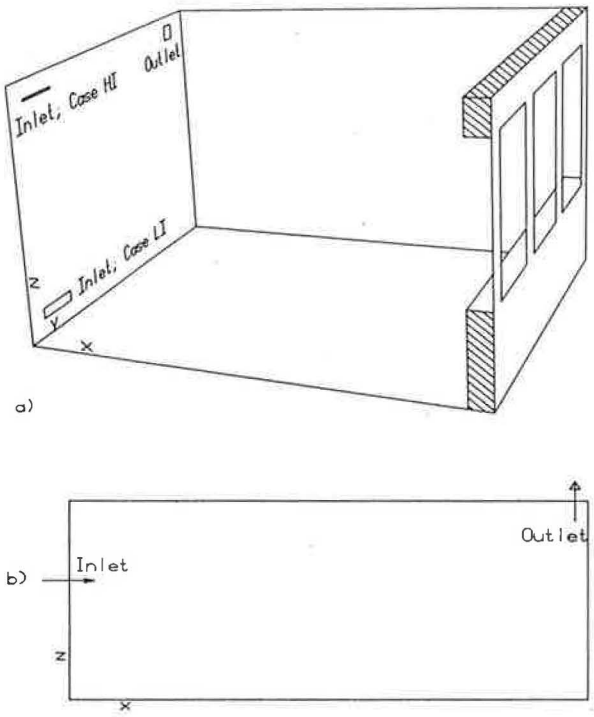

Fig. 1. Flow configurations. (a) Cases HI and LI. (b) Case 2D.

the local purging flow rate numerically. The local mean age is calculated for every cell, which means any number of cells between, for example, 2000 and 8000 for a three-dimensional room. Because this number is considerably higher than anything done experimentally (e.g. measurements at five stations [3]), a much more complete picture of the age distribution can be obtained when the flow is numerically simulated than from previous experimental investigations. The distribution of the local mean age has been calculated in two three-dimensional, buoyantly ventilated rooms in which the temperature and the local mean age were measured [3]. In one of the cases (Fig. 1a) the inlet and the outlet are situated near the ceiling (hereafter denoted by Case HI; high inlet). The incoming air was warmer than that of the room and the windows were cold, simulating a ventilation situation in winter. This configuration was expected to give a very poor ventilation with high average mean age for the room. In the other case (see Fig. 1a) the inlet was placed near the floor (hereafter denoted by LI; low inlet) and the outlet was situated near the ceiling as in Case HI. The incoming air was colder than the air in the room and the windows were warm, simulating a ventilation situation in summer. This configuration was expected to give low average local mean age for the room.

As there does not yet exist an experimental method for measuring the local purging flow rate, it is expected that a numerical simulation of the field of local purging flow rate might enhance the understanding of the concept and give an idea of its future use and application. It is very expensive to calculate the local purging flow rate since a separate calculation has to be made for each cell involved. For this reason, the local purging rate field was calculated in a two-dimensional iso-thermally ventilated room (hereafter denoted by Case 2D, see Fig. 1b) in which the flow field was measured [4]; the local mean age field was also calculated for this case. For calculating the flow field in this room, a new one-equation turbulence model [5] was used.

Since both the local mean age and the local purging flow rate can be simulated, numerically as well as experimentally (at least in theory), by using passive contaminants, the flow field can be calculated first without introducing any contaminants. The obtained flow field can then be used when calculating the local mean age and the local purging flow rate, introducing passive contaminants as appropriate.

In the following section the programs that have been used in the calculations, the boundary conditions and the new one-equation turbulence model are described. The mean age and the local purging flow rate are discussed in Section 3, and expressions from which they are calculated are derived or given. Results are presented and discussed in Section 4 and in the last section conclusions are drawn.

2. SOLUTION PROCEDURE

The PHOENICS computer program [6] has been used (see also [7]) for the three-dimensional calculations and a slightly modified version of TEACH-T [8] for the two-dimensional calculations. These programs solve equations of the type

$$\frac{\partial}{\partial \tau}(\rho\phi)+\frac{\partial}{\partial x_i}\left(\rho U_i\phi-\Gamma_\phi\frac{\partial \phi}{\partial x_i}\right)=S_\phi \qquad (1)$$

by expressing them in finite difference form. The finite difference equations are solved by a procedure which is based on the SIMPLE procedure [9] (see also e.g. [10]). The four main features are staggered grids for the velocities; formulation of the difference equations in implicit, conservative form, using hybrid upwind/central differencing; rewriting of the continuity equation into an equation for the pressure correction; and iterative solving of the equations.

In the present calculations the dependent variable in Eq. (1) takes the forms: U, V, W, t, k, ε, c and 1 (continuity equation). The corresponding coefficients, Γ_ϕ, and sources, S_ϕ, are defined in Table 1.

For Case 2D a new one-equation turbulence model was used, which has previously been tested in parabolic flows [5] and in elliptical flows [11] with good results. In this model the turbulent length scale L_t is calculated from

$$L_{t,i}=\kappa \exp\left(-1.0\, n_i/\delta_i\right)k^{1/2}\int_{n_{i,p}}^{n_i} k^{-1/2}\,\mathrm{d}n_i+\kappa n_{i,p}, \qquad (2a)$$

where n_i is the normal coordinate from wall 'i', δ_i is half the length of the room in n_i-direction and subscript 'p' denotes a point within the inertial sublayer near the wall (for further details, see [5]). L_t is then taken as the minimum of all four $L_{t,i}$, in other words,

$$L_t=\min\left\{L_{t,x=0},\ L_{t,x=1},\ L_{t,z=0},\ L_{t,z=H}\right\}. \qquad (2b)$$

Along with this length-scale equation, the k-equation was used. The dissipation term in the k-equation was

Table 1. Definition of Γ_ϕ and S_ϕ for conservation equations solved

Equation	ϕ	Γ_ϕ	S_ϕ*
Continuity	1	0	0
Momentum	U	μ_{eff}	$-\partial p/\partial x$
Momentum	V	μ_{eff}	$-\partial p/\partial y$
Momentum	W	μ_{eff}	$-\partial p/\partial z+\rho g(t-t_{\text{ref}})/(t_{\text{ref}}+273)$
Temperature	t	$\mu_{\text{eff}}/\sigma_t$	0
Turbulence energy	k	$\mu_{\text{eff}}/\sigma_k$	$G-\rho\varepsilon+G_B$
Turb. dissipation	ε	$\mu_{\text{eff}}/\sigma_\varepsilon$	$\varepsilon/k(C_{1\varepsilon}G-C_{2\varepsilon}\rho\varepsilon)$
Concentration	c	$\mu_{\text{eff}}/\sigma_c$	0

* $G \equiv \mu_{\text{eff}}\dfrac{\partial U_i}{\partial x_j}\left(\dfrac{\partial U_i}{\partial x_j}+\dfrac{\partial U_j}{\partial x_i}\right)$; $G_B \equiv -\dfrac{g}{\sigma_t}\dfrac{\mu_t}{t_{\text{ref}}+273}\dfrac{\partial t}{\partial z}$; $\mu_{\text{eff}} = \mu+\mu_t = \mu+C_\mu\rho k^2/\varepsilon$.

Constants [12]: $C_\mu = 0.09$; $C_{1\varepsilon} = 1.44$; $C_{2\varepsilon} = 1.92$; $\sigma_k = 1.0$; $\sigma_\varepsilon = 1.3$; $\sigma_t = 0.7$; $\sigma_c = 0.7$.

calculated as $C_D k^{3/2}/L_t$ and the turbulent viscosity was calculated as $\mu_t = C'_\mu\rho k^{1/2}L_t$ ($C_D = 0.1643$; $C'_\mu = 0.5478$).

Boundary conditions

Geometrical and boundary data are given for the three configurations in Table 2. Wall functions of conventional type are used [13, 14]. The temperature at the walls and the windows were prescribed according to experimental data [3]. The temperatures at the walls were all set to values close to 20°C in the two non-isothermal cases. At the outlet the exit velocity was calculated from mass balance and zero streamwise gradient was imposed on the rest of the variables.

When the dimensions of the inlet are small it is preferable to prescribe the velocities in a box which encloses the inlet. This procedure, chosen by several authors including [15–18] allows an economical resolution of the jet-like flow emanating from the inlet. In all the works cited above relevant experimental data have been available; in the present work no such experimental data exist for the three-dimensional calculations, and for Case 2D this procedure turned out to be inappropriate. Preliminary calculations (for Case 2D) showed that, using this procedure, the reattachment of the jet to the upper wall (see Fig. 1b) was predicted too far from the inlet compared with experimental data. This procedure was consequently abandoned and the inlet was represented by only one cell, giving better agreement with experimental data; it was necessary, however, to prescribe the turbulent viscosity in the jet. The reason for this is that the one-equation turbulence model is inadequate in free jet flows. For the three-dimensional calculations, the calculation of the flow was divided into two steps: first the flow in a box enclosing the inlet was calculated; then the flow in the room was calculated using the obtained results to prescribe all variables, except the temperature, at three planes inside the box. See [14] for more details.

Table 2. Boundary conditions and geometrical data

Case	2D	HI	LI
L	4.0	4.2	4.2
H	2.0	2.5	2.5
B	—	3.6	3.6
h	0.006	0.0155	0.1
b	—	0.5	0.467
y_{in}	—	3.1	3.1
z_{in}	1.2	2.3	0.23
U_{in}	3.0	2.61	0.45
W_{in}	—	0.7	—
Q (m³/h)	64.8	75.6	75.6
τ_n (h)	0.12	0.5	0.5
t_{in}	—	32	15
t_{window}	—	14	29

3. THE CONCEPT OF MEAN AGE AND LOCAL PURGING FLOW RATE

The concept of mean age and of local purging flow rate has been thoroughly treated [1, 2]. The mean age of the air at a point (= *local* mean age) is the time that has elapsed (on average) since the molecules passing this point entered the room. The word 'mean' refers here to the mean age of the molecules and from here on 'mean' will be omitted and the 'age' will be used instead of the formally more correct term, 'mean age'. There are two, perfectly equivalent, methods of obtaining, numerically or experimentally, the local age: (i) Step-up, at time $\tau = 0$ a fraction of the supplied air is labelled with contaminant and the concentration of contaminant is measured at the point(s) in the system (room) where the local age is to be obtained. (ii) Step-down, the system (room) is initially filled with a known homogenous concentration of contaminant and is then supplied with 'fresh' air (no contaminant); the decay of concentration is recorded at the point(s) where the local age is to be obtained.

The equation for the local age in a step-up simulation is now derived. At time $\tau = 0$ a fraction, c_0, of all the entering molecules in the system are labelled. Consider an arbitrary point (control volume) P within the system at time τ where the concentration is $c_P(\tau)$. A fraction $c_P(\tau)/c_0$ of the molecules at point P thus have an age less or equal τ. Since $c_P(\tau)/c_0$ has the characteristics of a cumulative distribution function, $\phi_P(\tau) = c_P(\tau)/c_0$ is defined as the cumulative distribution function of the local age at point P. φ denotes the probability density function (also called frequency function) for the age, and is defined as $\varphi = \partial\phi/\partial\tau$ (see any introductory text book on statistics, e.g. [19]). The local age, $\bar{\tau}_P$, can then be

calculated as

$$\bar{\tau}_P = \int_0^\infty \tau_P \varphi_P(\tau)\,\mathrm{d}\tau = \int_0^\infty \tau_P \hat{c}\phi_P(\tau)/\partial\tau\,\mathrm{d}\tau$$

$$= [\tau_P(\phi_P - 1]_0^\infty - \int_0^\infty (\phi_P(\tau) - 1)\,\mathrm{d}\tau$$

$$= \int_0^\infty (1-\phi_P(\tau))\,\mathrm{d}\tau = \int_0^\infty (1 - c_P(\tau)/c_0)\,\mathrm{d}\tau. \qquad (3a)$$

The first expression on the RHS of Eq. (3a) is given by statistics theory [19]. The third expression is obtained by partial integration, using $\phi_P - 1$ as a primitive function of $\hat{c}\phi_P/\hat{c}\tau$, and where the term in square brackets is zero since $\phi_P(\infty) = 1$.

For a step-down simulation one gets $\phi_P(\tau) = 1 - c_P(\tau)/c_0$ which, by use of Eq. (3a), gives

$$\bar{\tau}_P = \int_0^\infty (1-\phi_P(\tau))\,\mathrm{d}\tau = \frac{1}{c_0}\int_0^\infty c_P(\tau)\,\mathrm{d}\tau. \qquad (3b)$$

The average age of the system (room) can be calculated either as

$$\bar{\tau} = \frac{1}{V}\int_V \bar{\tau}_P\,\mathrm{d}V \qquad (4a)$$

or from the first moment of the concentration curve at the exit point normalized by the corresponding zero moment

$$\bar{\tau} = \int_0^\infty c_e(\tau)\tau_e\,\mathrm{d}\tau \Big/ \int_0^\infty c_e(\tau)\,\mathrm{d}\tau. \qquad (4b)$$

It may be mentioned that the theory gives that $\bar{\tau}_e/\tau_n = 1$ [1], [2]. In the present work a step-down simulation was used. It is not necessary to carry out the integration in Eq. (3b) from $\tau = 0$ to ∞. Since the concentration after some time decays exponentially $[c_P(\tau)/c_0 = \exp(-\lambda\tau)]$, the calculations were stopped when the slope λ had reached a constant value (at time τ_i) and the integral from τ_i to ∞ was calculated as $c_P(\tau_i)/(\lambda c_0)$.

The age can be obtained directly from a transport equation as a steady state solution of Eq. (1) with $\phi = \bar{\tau}_P$ and $S_{\tau_P} = 1$ (i.e. homogenous source) [2]. The age was calculated in this way for Case 2D and the obtained age-field was indeed the same as that obtained from Eq. (3b).

The concept of the local purging flow rate, U_P, can be understood as the net rate at which a dynamically passive contaminant is 'flushed' out of the system from a point P, or, equivalently, the rate at which fresh air is supplied to a point P, where P is an arbitrary point within the system. Since the calculation domains (rooms) are divided into control volumes (i.e. non-continuous systems) it is preferable to refer to a control volume P, dividing the non-continuous systems into vessels or compartments [20], rather than to a point P. The local purging flow rate is obtained, numerically or experimentally (at least in theory, see Section 1), by introducing a source of a dynamically passive contaminant at an arbitrary control volume P where U_P is to be obtained. An expression for U_P is easily obtained by setting up a mass balance for the contaminant. If a source $\dot{m}_P$ of contaminant is placed at control volume P, then $\dot{m}_P$ must also, as demanded by continuity when steady state has been reached, exit the system, which gives $\dot{m}_P = Qc_e$. $\dot{m}_P$ is obtained from the definition of U_P as $\dot{m}_P = U_P c_P$, so that

$$U_P = \dot{m}_P/c_P = Q\frac{c_e}{c_P}. \qquad (5)$$

In order to get a further understanding of the physical meaning of U_P let P be a control volume situated in a stagnant region. The concentration at P will then be high and, according to Eq. (5), the local purging flow rate low ($\dot{m}_P$ kept constant). The opposite, i.e. low c_P and high U_P, will be the case when P is situated in a well ventilated region. It may be noted that Q and U_P have the same units, namely [m^3/s] or [kg/s].

Both the age and the local purging flow rate fields are simulated using dynamically passive contaminants, which means that the flow field is not influenced by the contaminants. This makes it possible to calculate the flow field first and then use this calculated flow field in the calculations of the age and U_P. As pointed out in Section 1, it is computationally very expensive to calculate the field of the local purging flow rate, since a separate calculation has to be made for each control volume at which U_P is to be obtained by introducing a source of contaminant. This is the reason why the U_P-field has been calculated in a two-dimensional rather than in a three-dimensional room; the number of cells, and consequently also the number of separate calculations, is, for example, reduced to 500 in a two-dimensional calculation from 5000 in a three-dimensional one.

The concentration equation is linear since the contaminant is dynamically passive, which means that the fields of velocity and the exchange coefficient for the concentration appear as constants in the concentration equation. This means further that U_P calculated from Eq. (5) is independent of the size of $\dot{m}_P$.

Since the calculated U_P is dependent on the size and form of the control volume P where $\dot{m}_P$ is introduced (see Appendix) a uniform grid should be used, i.e. all control volume sides should be of equal length. Using quadratic control volumes of equal size would mean that every control volume side would be of length 0.006 m, which is the height of the inlet in Case 2D; 222 000 nodes would then be needed to cover the calculation domain, which is clearly unrealistic. In the present work the flow field was calculated using unequally spaced grid lines. When the U_P-field was calculated two grids with control volume sides equal to 0.05 and 0.1 m, respectively, were used. The velocity field for these 'U_P-grids' was obtained by interpolation from the 'velocity grid' so as to satisfy continuity. For comparison, the U_P-field was also calculated using the 'velocity' grid.

4. RESULTS

Three-dimensional calculations

A numerical grid with $15 \times 14 \times 12$ nodes was used in both cases; in Case LI a grid with $21 \times 21 \times 18$ nodes (hereafter denoted by Case LI21) was also tested. In the latter case the special inlet procedure was abandoned since it was considered that a sufficient number of nodes were situated near the inlet to enable a proper description

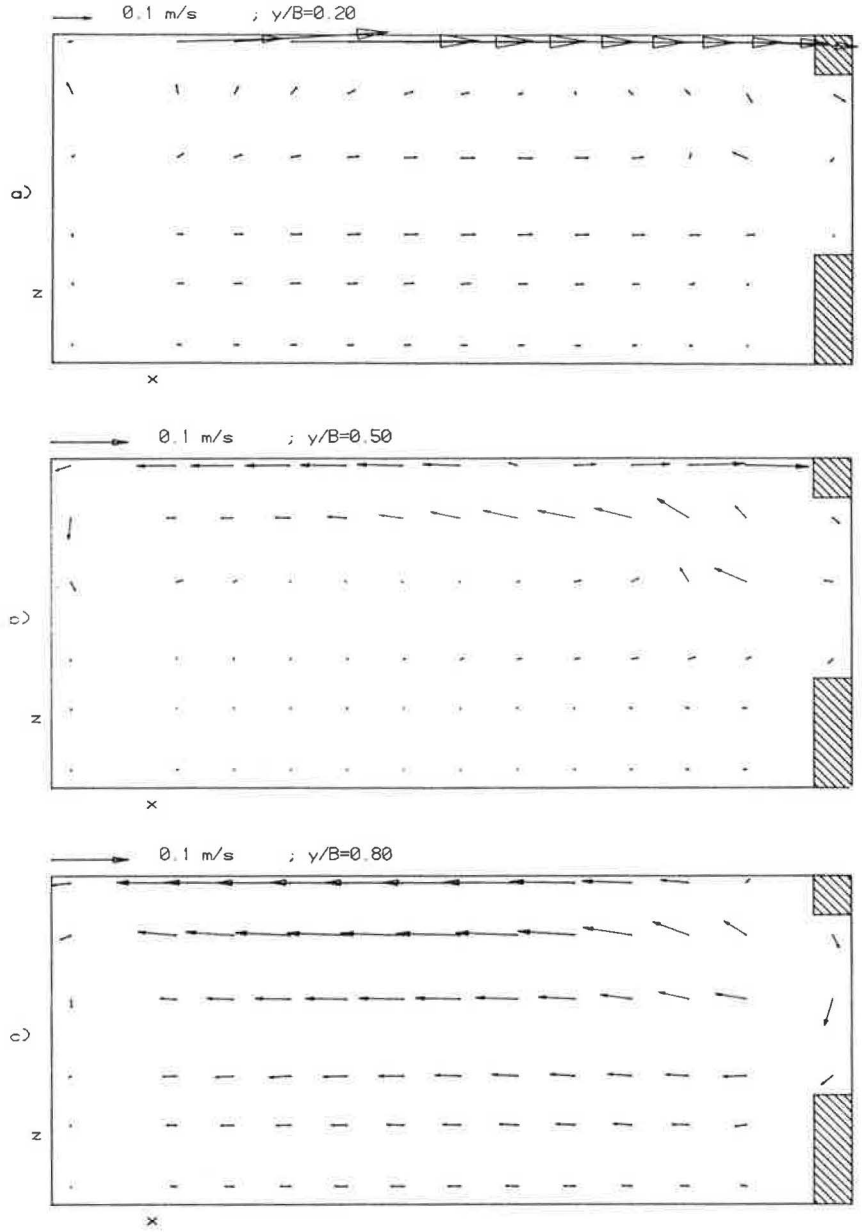

Fig. 2. Calculated velocity vectors. Case HI.

of the steep velocity gradients prevailing there; the inlet was represented by 20 grid nodes. The results obtained with the $21 \times 21 \times 18$ nodes grid did not differ much from those obtained with the $15 \times 14 \times 12$ nodes grid [14]. The results presented below have been calculated using the latter grid.

In Figs 2 and 3 velocity vectors for Case HI are drawn. From these plots it can be seen that the wall jet following the ceiling hits the wall opposite the inlet and that the flow is forced along this wall. The flow does not fall down towards the floor because of the upwards directed buoyancy force. It reaches the side wall at $y = B$ and turns left towards the outlet. This large counter-clockwise vortex near the ceiling is spread by friction in the whole room: the result is a counter-clockwise vortex at each z-level, with little fluid being interchanged between the different z-levels.

When calculating the local age field, a time step $\Delta\tau = 30$ was chosen; 15 s was also tested but it gave the same result as $\Delta\tau = 30$ s. The decay of the concentration was found to be exponential for the whole field (i.e. λ is a constant, see Section 3) after 20–40 min ($0.67\tau_n$ to $1.33\ \tau_n$) in real time, depending on the problem. The calculations were consequently stopped at this stage and the remainder of the integral in Eq. (3b) was calculated as $c_P(\tau_i)/(\lambda c_0)$ (see Section 3).

The flow pattern in Figs 2 and 3 results in high local age near the floor and gradually lower the $\bar{\tau}_P$ near the ceiling as is clearly recognizable in Figs 4 and 5. Experimental data obtained by Sandberg [3] are shown in Fig. 4b. The accordance between predictions and experimental data is not very good, with local discrepancies up to 25%. While numerical predictions show an almost monotonic increase in age of the air with decreasing z,

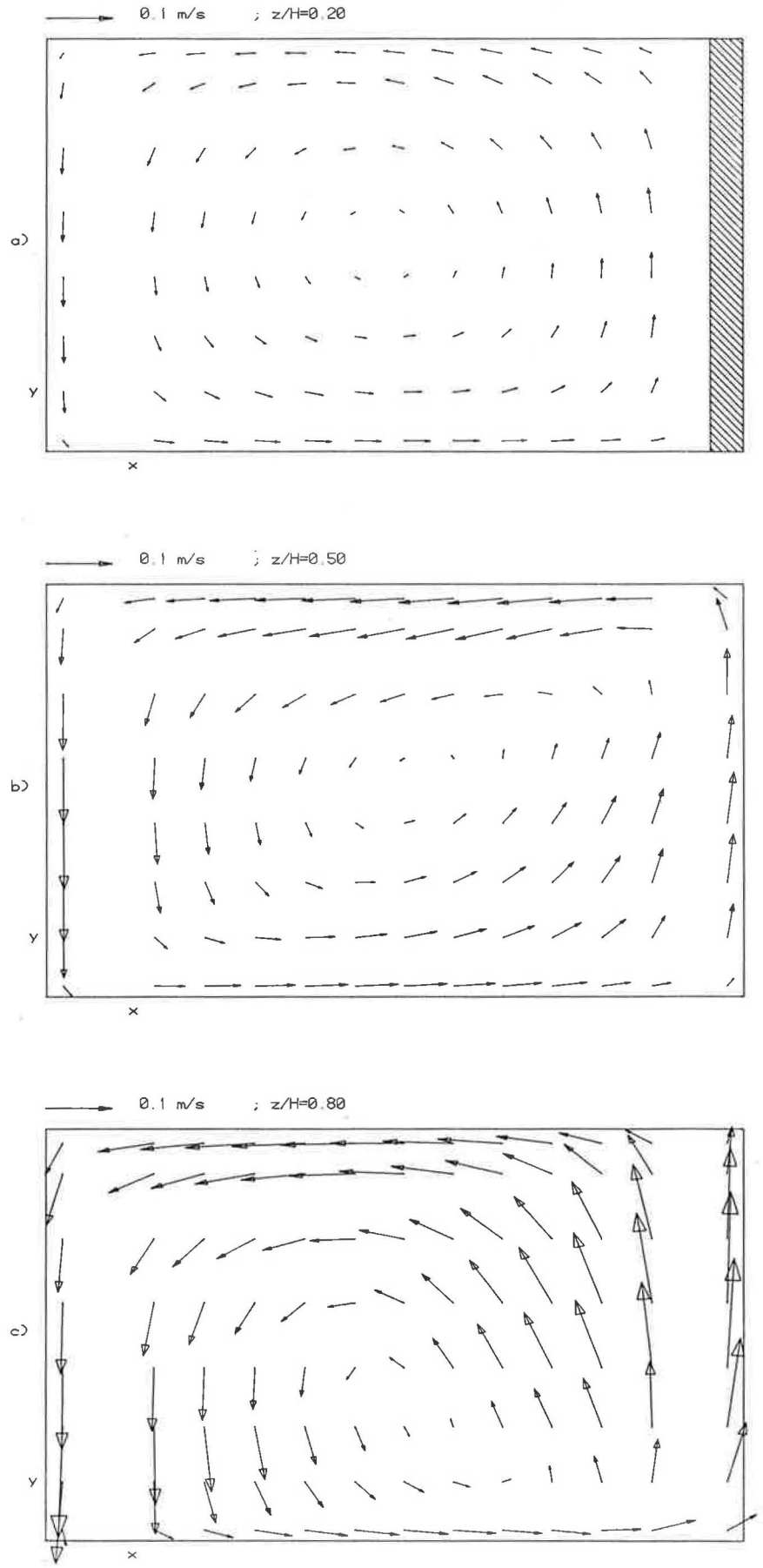

Fig. 3. Calculated velocity vectors. Case H1.

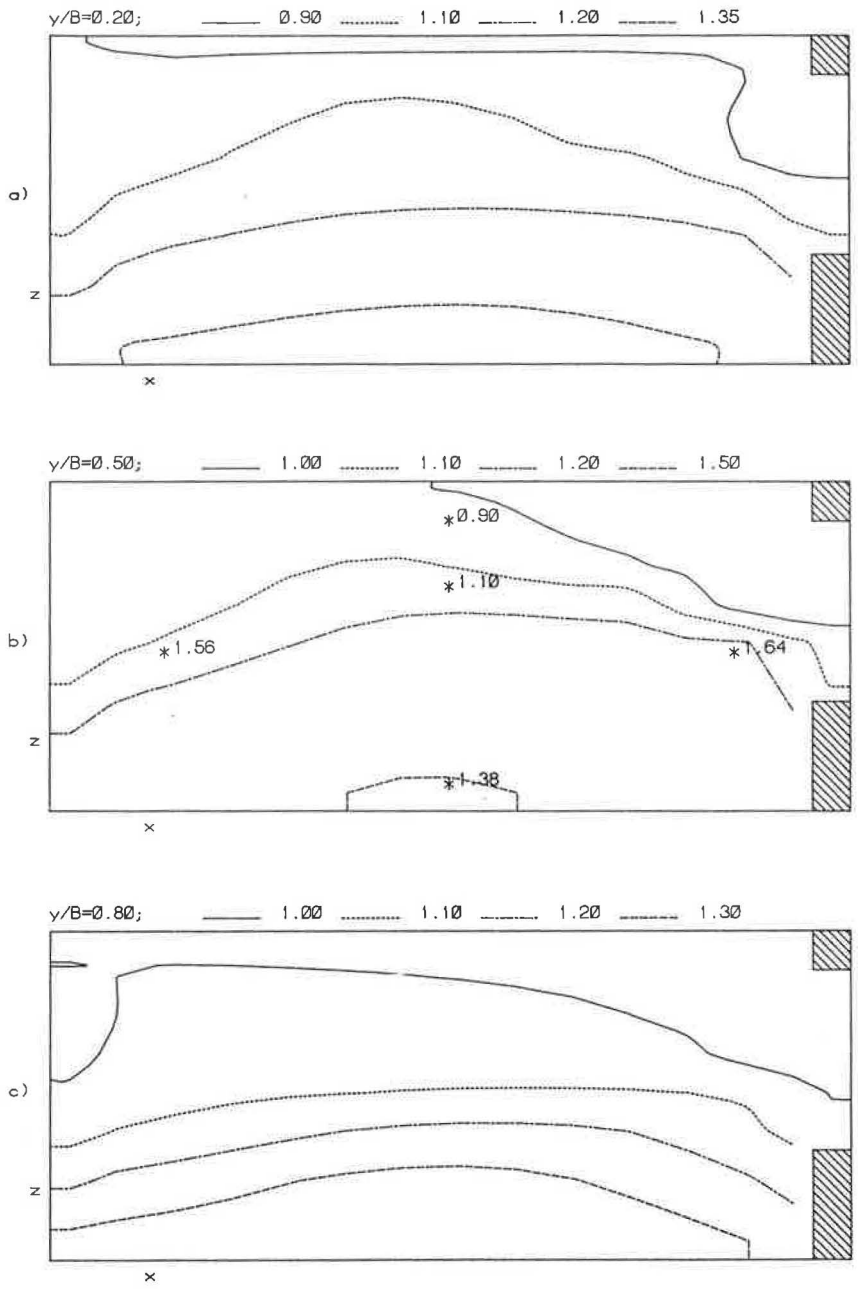

Fig. 4. Predicted contours of local age scaled with τ_n. Case HI. Expts by Sandberg [3] at stations marked with an asterix.

the experiments show maximum age in the middle (in the z-direction, that is) of the room. This may indicate that the predicted flow pattern is more stratified than that in the experiments. The average age for the room was calculated from Eq. (4a) to be $\bar{\tau}/\tau_n = 1.14$; the corresponding value in the experiments, from Eq. (4b), was 1.3. The predicted average age of the air in the room is thus fairly well in accordance with the experimental value. The temperature field was also measured by Sandberg [3]. The predicted temperatures are between 1 and 2 C too high compared with the experimental values; the temperature gradient, which influences the velocity field through the buoyancy term is, however, rather well predicted. G_B was set to zero because the predicted age field with $G_B = 0$ was closer to experimental data than when G_B was included [14].

Velocity vectors for Case LI are shown in Figs 6 and 7; the flow pattern is much more complicated here than in Case HI because the flow can not find a short convenient way out of the room. The result is a much better ventilation situation with lower average age of the air in the room. The air coming from the inlet falls down to the floor—due to the coanda effect and to the downwards directed buoyancy force—goes towards the wall opposite the inlet and successively turns, as this wall is approached, to the left. This counter-clockwise vortex does not spread to the flow in the rest of the room, as it does in Case HI. Quite the opposite is in fact the case: the flow above the

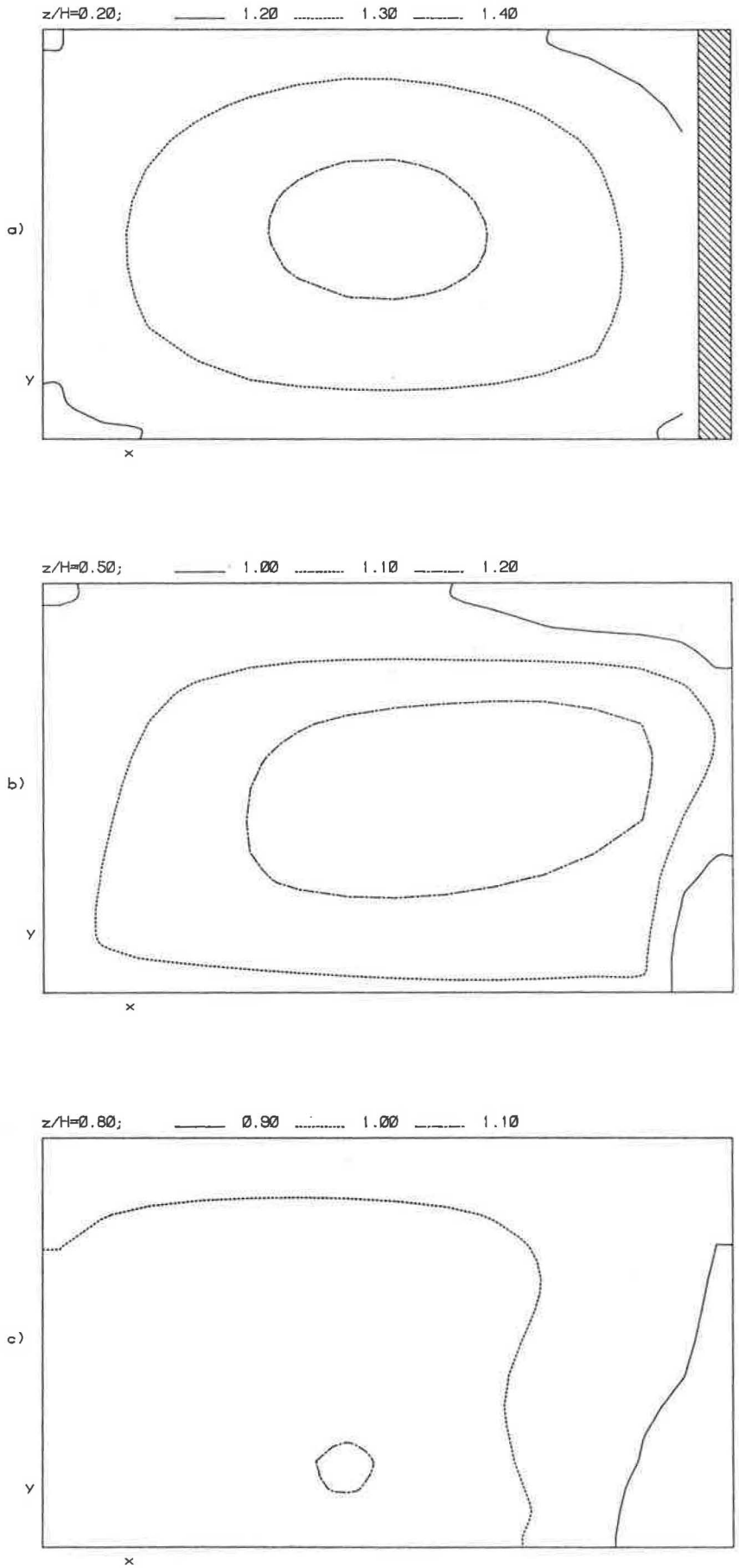

Fig. 5. Predicted contours of local age scaled with τ_n. Case H1.

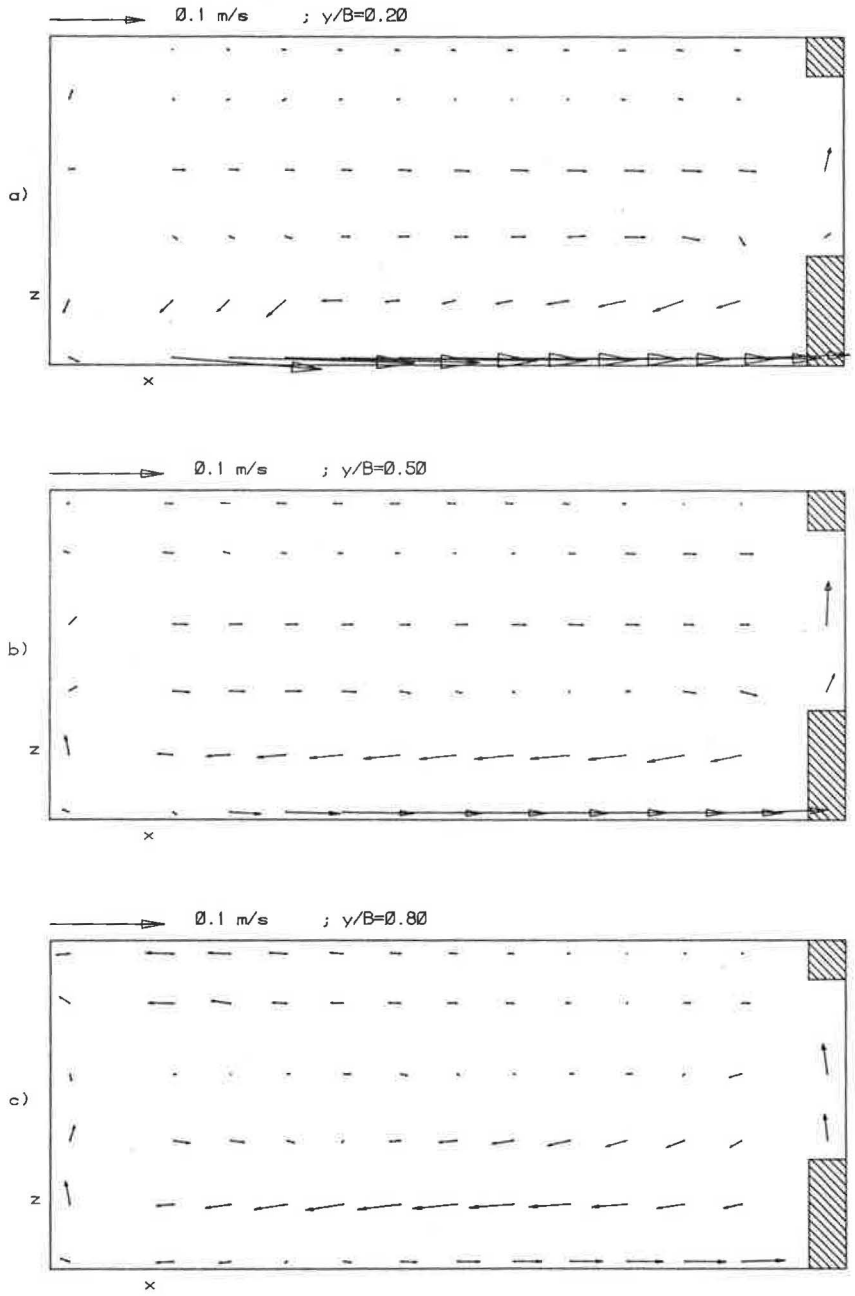

Fig. 6. Calculated velocity vectors. Case LI.

vortex near the floor is in the opposite direction. The predicted temperatures are 1–2°C lower than experimental data; the discrepancies are of the same order as in Case HI (see above). The temperature gradient is, however, rather well predicted.

The distribution of the local age is shown for Case LI in Figs 8 and 9. The predicted local age field is compared with experimental data in Fig. 8b; the agreement is not very good. In particular, the experimental value $\bar{\tau}_p/\tau_n = 0.2$ near the floor is overpredicted by 150%; this is surprising since regions near the inlet should be well predicted. As can be seen in the vector plot of the velocity field in Figs 6 and 7, this point is almost hit by the primary jet which should make the predictions of this area especially exact. The discrepancy between predicted and experimental local age near the floor might be explained by either too coarse a grid, or the predicted turbulent diffusion being too high which would cause too effective a mixing and which would smooth out concentration gradients. The former explanation does not seem very likely as the predicted local age at this point is almost the same in Case LI and Case LI21. Against both explanations it can be further argued that works carried out previously show good agreement between calculated and experimentally obtained concentration fields (see e.g. [21–23]). The third explanation could be that the experimental value is somewhat too low. It is likely that the reason for the discrepancies between numerical and

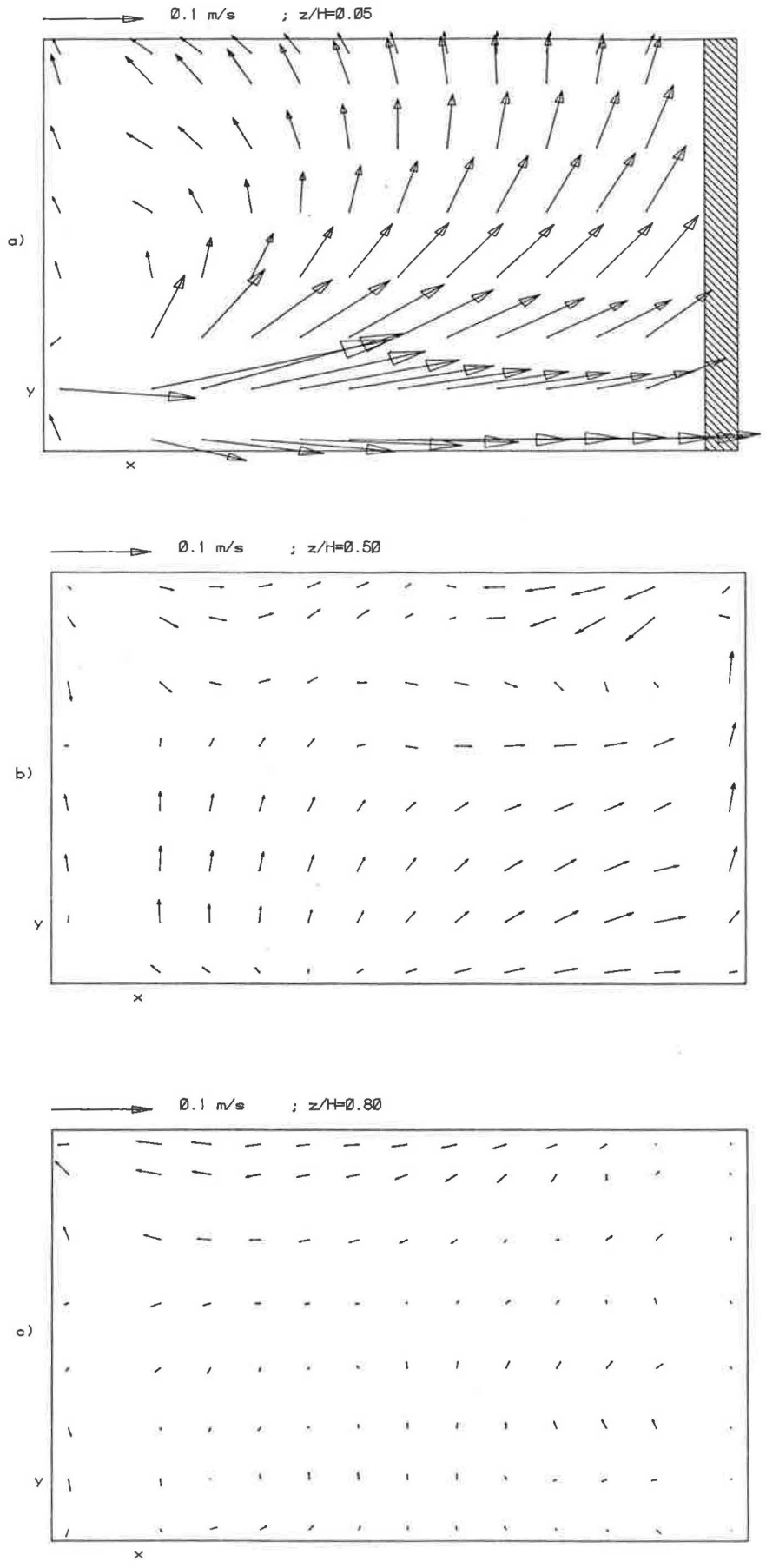

Fig. 7. Calculated velocity vectors. Case LI.

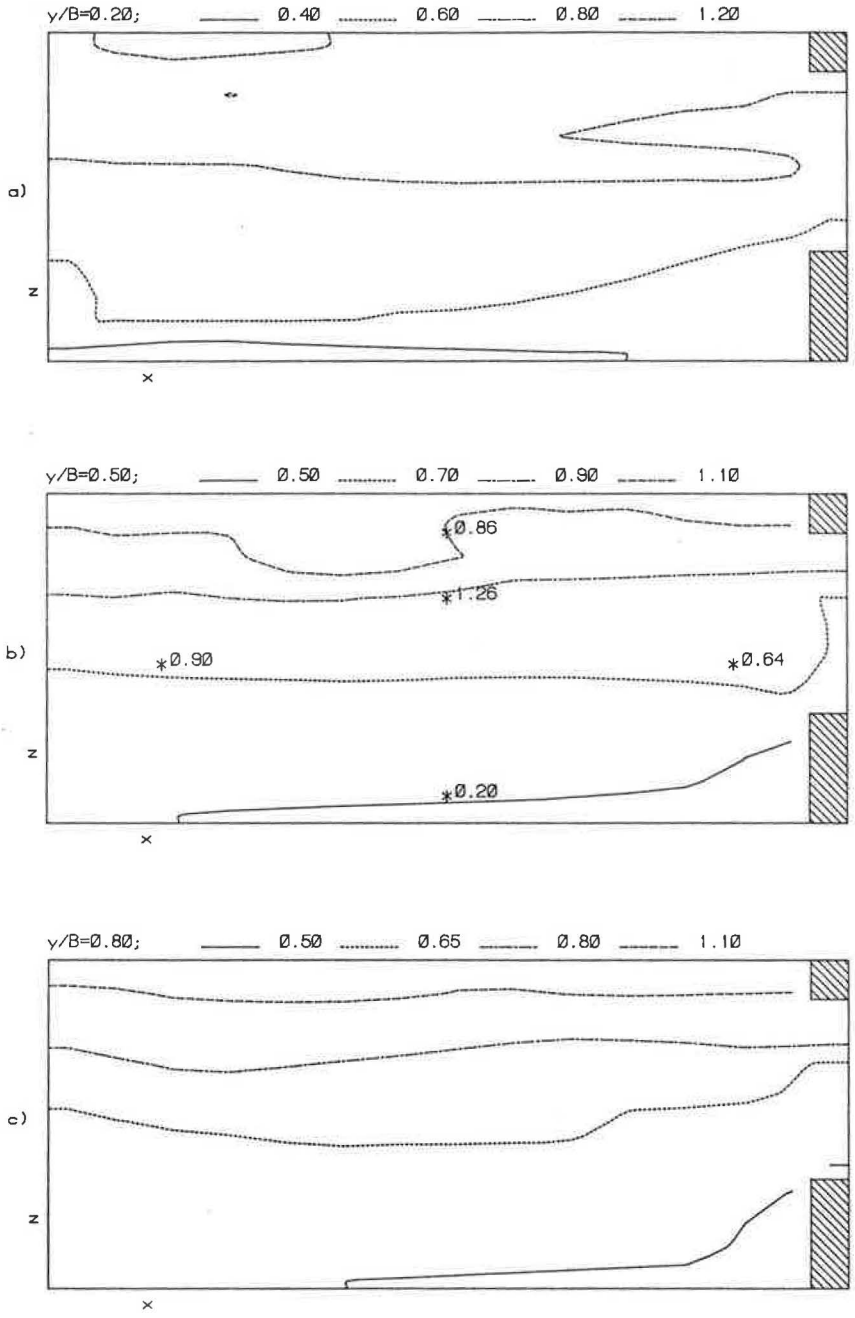

Fig. 8. Predicted contours of local age scaled with τ_n. Case LI. Expts by Sandberg [3] at stations marked with an asterix.

experimental results is to be found in a combination of the explanations above (and below). The predicted average age of the room is, however, well predicted; $\bar{\tau}/\tau_n = 0.75$ and $\bar{\tau}/\tau_n = 0.73$ for Cases LI and LI21, respectively, both to be compared with the experimental value 0.66.

Various discrepancies between predictions and experimental data have been mentioned above. One major source of error, which could explain many of the discrepancies, is probably the velocity field. The turbulence model and the wall functions are known to be, at their best, sufficient for engineering purposes in three-dimensional, elliptical buoyant flow calculations. Hjerthager [17] has calculated the flow in a three-dimensional, buoyant ventilated room and compared the results with experimental data; the agreement with these data was, in some regions, moderate. When searching to explain discrepancies between predictions and experimental data, it should not be forgotten that the latter also contain some errors, e.g. some uncertainty in the boundary values at the inlet, incomplete homogenous mixing of the contaminant in the initial transient (see [3]). Another source of error may be that when the decay of the concentration was measured in order to obtain the age, the experiments were carried out once only, whereas perhaps they should have been carried out a number of times in order to form

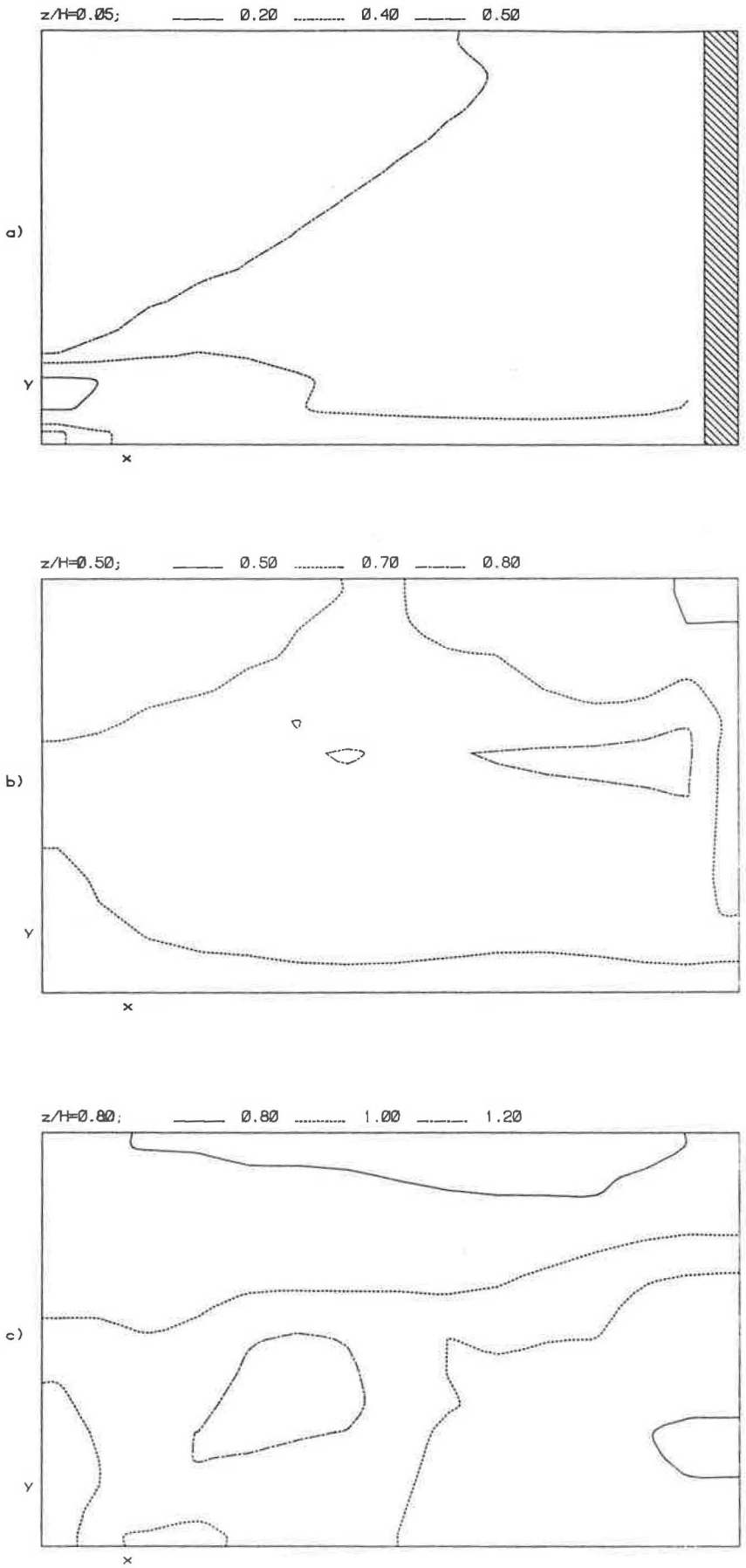

Fig. 9. Predicted contours of local age scaled with τ_n. Case L1.

ensemble averages (M. Sandberg, personal communication). It should also be mentioned that when the calculated velocity field is studied, the calculated local age fields seem very reasonable. This has indeed been the object of the present work : to show that from a calculated velocity field the age distribution can be calculated.

All calculations were carried out on a VAX-750 machine. The required CPU time to get a converged solution, i.e. when the residuals (scaled with the total incoming flux of the relevant variable) for all equations had become less than one percent, was as follows: inlet-box calculations (5 h), flow field calculations for Cases HI, LI and LI21 (6, 6 and 38 h), calculations of the age field for Cases HI, LI and LI21 (3, 3, 15 h).

Two-dimensional calculations

The grid used in these calculations was of size 28×22; calculations were also made with a grid with 42×35 nodes. The flow patterns predicted using the two different grids are almost identical; the velocity contours are slightly better predicted when the 42×35 grid is used. The predictions obtained using the 28×22 grid are, however, quite adequate for engineering purposes. The predicted results shown in the following figures have been obtained using the 42×35 grid. In Figs 10 and 11 predicted velocity vectors and velocity contours are compared with experimental data obtained by Åkesson [4]. The agreement between predictions and experiments is good, which indicates that the one-equation turbulence model of Davidson [5] is adequate for numerical predictions of the flow in two-dimensional, isothermally ventilated rooms. A recirculation zone appears in the experiments in the lower left corner of the room which does not appear in the predictions; this discrepancy may be due to the rather large three-dimensional effects in the experiments in this region. It should be mentioned that the computational effort for solving the flow field was reduced by 60% using the one-equation turbulence model compared with when the k-ε turbulence model was used.

Time steps of 30 s were used when the local age field was calculated; $\Delta\tau = 10$ s was also tested but it gave the same results. At time $\tau = 5$ min ($=0.7\ \tau_n$), λ was found to become constant (see Section 3) and the calculations were consequently stopped. The predicted local age is shown in Fig. 12; as expected, the local age has higher values near the floor and has its highest values under the inlet. Figure 13 shows the predicted local purging flow rate. Figures 13a and 13b show the predicted U_P-field using the equal spacing (0.1 and 0.05 m, respectively) of grid lines; the predicted U_P-field in Fig. 13c is obtained using the 'velocity grid' (see Section 3). The general features of the U_P-field in Fig. 13 are the same which shows that the calculated U_P-field is not too sensitive to the choice of grid, provided that δ is given reasonable size (see Appendix). It is seen that the predicted U_P-fields in Figs 13a and 13c are very similar in the lower part of the room, whereas the predicted U_P-field in the upper region in Fig. 13c is similar to that in Fig. 13b. The explanations for this is that for the grid in Fig. 13c $\delta y = 0.1$ in the lower part of the room, and $\delta y = 0.05$ in the upper part. It may be noted that $U_P/Q \neq 1$ at the outlet in Fig. 13 (not noticeable in Fig. 13a). This is because the outlet is covered by more than one control volume; the more control volumes the outlet is covered by, the lower the calculated U_P (see Appendix). This is also the case at the inlet. It should thus be kept in mind that the calculated U_P-field at the oulet and the inlet is especially grid dependent.

Comparing the local age field and the local purging flow rate field, it may be concluded that the main features

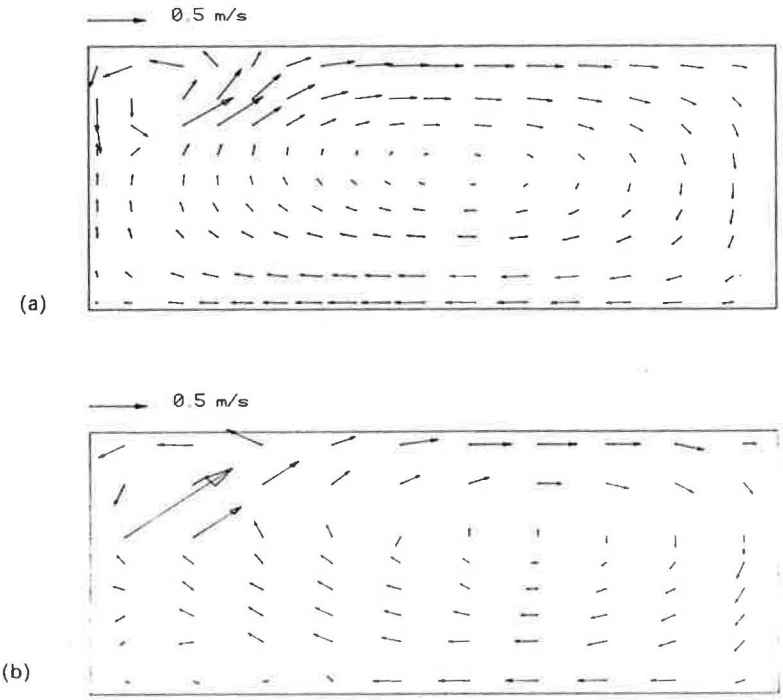

Fig. 10. Velocity vectors. Case 2D. (a) Predictions. (b) Experiments by Åkesson [4].

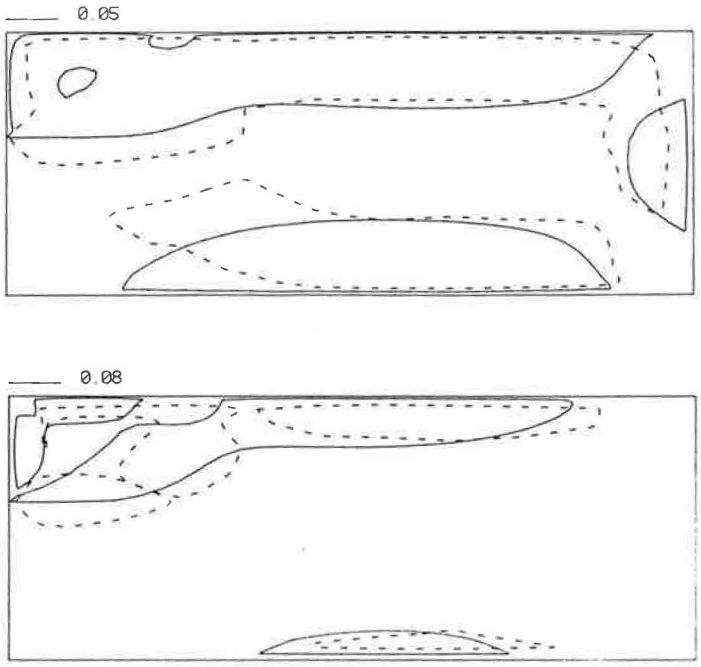

Fig. 11. Contours of the absolute velocity scaled with U_{in}. Solid lines: predictions. Dashed lines: expts by Åkesson [4]. Case 2D.

of the ventilation situation are shown by either of the two fields; they both indicate that the flow in the lower half of the room is more stagnant than in the upper half. The largest differences between the two fields occur in the regions near the two upper corners. In the region of the upper left corner the gradient of U_P is large: to the left of the point where the jet reattaches to the ceiling (where the flow when reaching the ceiling turns back towards the inlet wall, see Fig. 10) low values prevail, while to the right of this point (where the flow goes more directly towards the outlet) U_P has higher values; the age of the air is low since it does not take a long time for the air to reach the region near this corner. Below the outlet, where the flow is directed from the outlet, U_P attains low values whereas the air here is not very 'old'.

Sandberg and Sjöberg [1] have proved, theoretically, that in regions where $\bar{\tau}_P/\tau_n > 1$ the product of U_P and $\bar{\tau}_P$ should be less than or equal to the volume of the room, i.e.

$$U_P\bar{\tau}_P \leqslant V, \quad \text{or,} \quad U_P/Q\bar{\tau}_P/\tau_n \leqslant 1; \quad \text{when} \quad \bar{\tau}_P/\tau_n > 1. \tag{6}$$

This relation restricts U_P more severely for higher values of $\bar{\tau}_P$. It should be remembered that the calculated U_P is dependent on the size of the control volume (see above and Appendix); the relation in Eq. (6) was, however, confirmed for all three grids in Fig. 13, but as the calculated $\bar{\tau}_P$ nowhere in the room is especially large ($\bar{\tau}_P \leqslant 1.1\ \tau_n$ everywhere) this confirmation is of little value. In order to 'prove' or 'disprove' the relation in Eq. (6) the local age field and the U_P-field should be calculated in ventilated rooms where regions of much higher values of $\bar{\tau}_P$ occur; the authors plan to do this in the near future.

For the two-dimensional calculations the required CPU times were as follows: flow-field calculations (coarse grid: 11 min, fine grid: 52 min), calculation of the age field (6 min), calculation of the U_P-field (2 h).

5. CONCLUSIONS

The local age field has been calculated in two three-dimensional buoyantly ventilated rooms, using computer programs utilizing finite-difference methods, and have

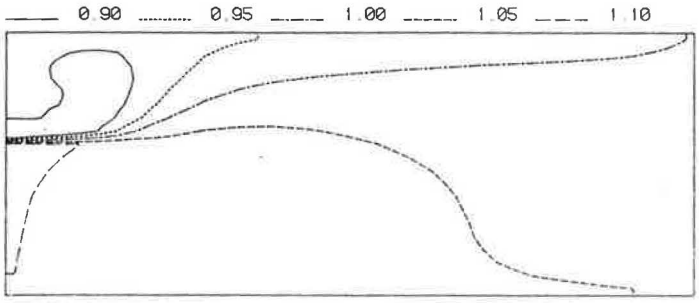

Fig. 12. Predicted contours of local age scaled with τ_n. Case 2D.

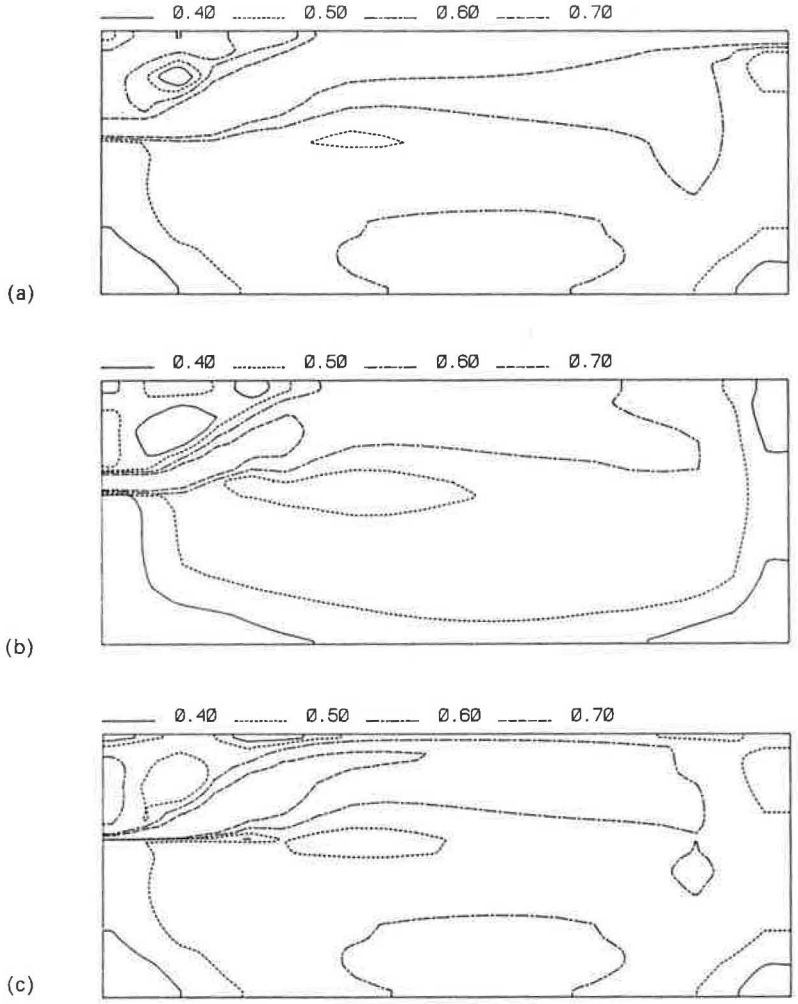

Fig. 13. Predicted contours of local purging flow rate scaled with Q. Case 2D. (a) 'U_P-grid'. $\delta = 0.1$ m. (b) 'U_P-grid'. $\delta = 0.05$ m. (c) 'Velocity-grid'.

been compared with experimental data. The local agreement is not very good, with discrepancies up to 25% (at one station 150%); the predicted average age of the rooms, being a measure of the 'global' ventilation situation, is rather well in agreement with experimental data (discrepancies of 12%). The rather large discrepancies between prediction and experiment are probably due to errors in predictions of the velocity field as well as uncertainties in the experiments; the predicted local age field seems, in view of the predicted velocity field, very reasonable. This was really one of the aims of the present work with respect to the local age field: to show that the local age field can be calculated when a velocity field has been calculated.

The flow in a two-dimensional isothermally ventilated room has been calculated using a new one-equation turbulence model developed by the first author. The predicted velocity field is well in agreement with experimental data, which indicates that the new one-equation turbulence model is appropriate when calculating these types of flows. The CPU time required for calculating the velocity field was reduced by 60% using this one-equation turbulence model compared with when the standard k-ε turbulence model was used.

The local age field and the local purging flow rate field have been calculated for this room. It was shown that the main features of the ventilation situation are readily obtained from either of these fields. It has been shown that the calculated U_P is dependent on the size of the control volume, δ; this dependence does not seem very severe provided that reasonable size on δ is chosen. A theoretical relation between the local age and the local purging flow rate field valid in regions of 'high' local age has been formulated by Sandberg and Sjöberg [1]. The predicted fields confirm this relation, but in order to 'prove' or 'disprove' this relation these fields should be calculated for ventilation situations where much higher values of the local age occur. The authors plan to undertake such numerical investigations in the near future.

Acknowledgements—This work has been carried out at the Department of Applied Thermodynamics and Fluid Mechanics, Chalmers University of Technology. The authors wish to thank Dr Mats Sandberg at the National Swedish Institute for Building Research, who has been very helpful and who initiated the work on the ventilation parameters. The Swedish Council for Building Research has sponsored this work.

REFERENCES

1. M. Sandberg and M. Sjöberg, The use of moments for assessing air quality. *Bldg Envir.* **18**, 181–197 (1983).
2. M. Sandberg, What is ventilation efficiency? *Bldg Envir.* **16**, 123–135 (1981).
3. M. Sandberg, TM 279 (in Swedish). Dept. of Heating and Ventilation, Royal Institute of Tech., Stockholm (1984).
4. K. Åkesson, Experimentell bestämning av hastighets- och temperaturfördelningen i en ventilerad lokal (in Swedish). Dept. of Applied Thermodynamics and Fluid Mechanics, Chalmers Univ. of Tech., Göteborg (1975).
5. L. Davidson, One-equation turbulence models in flows near walls, Rept. 86/1 2nd ed. Dept of Applied Thermodynamics and Fluid Mechanics, Chalmers Univ. of Tech., Göteborg (1986).
6. D. B. Spalding, A general purpose computer program for multi-dimensional one- and two-phase flow. Mathematics and Computers in Simulation, *IAMCS*, XXIII, 267–276 (1981).
7. H. I. Rosten and D. B. Spalding, PHOENICS-84 Reference Handbook. CHAM TR/100 (1985).
8. A. D. Gosman and F. J. K. Ideriah, TEACH-T: A general computer program for two-dimensional, turbulent, recirculating flows. Dept. of Mechanical Engineering, Imperial College, London (1976).
9. L. S. Caretto, A. D. Gosman, S. V. Patankar and D. B. Spalding, Two calculation procedures for steady, three-dimensional flows with recirculation. Proc. of the Third International Conference on Numerical Methods in Fluid Dynamics (J. Ehlers, K. Hepp, H. A. Weidemuller eds.), **11**, 60–68. Springer, Heidelberg (1972).
10. S. V. Patankar, *Numerical Heat Transfer and Fluid Flow*, McGraw-Hill, New York (1980).
11. L. Davidson and E. Olsson, Calculation of some parabolic and elliptic flows using a new one-equation turbulence model, to be presented at The 5th Int. Conf. on Numerical Methods in Laminar and Turbulent Flow, Montreal, Canada (1987).
12. B. E. Launder and D. B. Spalding, The numerical computation of turbulent flow. *Comp. Meth appl. Mech. Eng.* **3**, 269–289 (1974).
13. W. Rodi, *Turbulence Models and their Application in Hydraulics*. International Association of Hydraulic Research, Monograph, Delft, The Netherlands (1980).
14. L. Davidson, Turbulence modelling and calculation of ventilation parameters in ventilated rooms. Rept. 86/10, thesis, Dept. of Applied Thermodynamics and Fluid Mechanics, Chalmers Univ. of Tech., Göteborg (1986).
15. M. Larsson, Predictions of buoyancy influenced flow in ventilated industrial halls, Proceedings of Heat Transfer in Buildings, Dubrovnik (1977).
16. P. V. Nielsen, A. Restivo and J. H. Whitelaw, The velocity characteristics of ventilated rooms. *J. Fluid Engng.* **100**, 291–298 (1978).
17. B. H. Hjerthager, Flow, heat transfer and combustion in three-dimensional rectangular enclosures. Thesis, NTH, Trondheim (1979).
18. A. D. Gosman, P. V. Nielsen, A. Restivo and J. H. Whitelaw, The flow properties of rooms with small ventilation openings. *J. Fluid Engng.* **102**, 316–323 (1980).
19. G. R. Grimmett and D. R. Stirzaker, *Probability and Random Processes*. Clarendon Press, Oxford (1982).
20. Y. Zvirin and R. Shinnar, Interpretation of internal tracer experiments and local sojourn time distributions. *Int. J. Multiphase Flow* **2**, 495–520 (1976).
21. L. Davidson, Beräkning av hastighets- och concentrationsfältet i en tvådimensionellt ventilerad lokal med en intern föroreningskälla med hjälp av PHOENICS-koden (in Swedish). Rept. 83/7, Dept. of Applied Thermodynamics and Fluid Mechanics, Chalmers Univ. of Tech., Göteborg (1983).
22. S. Murakami, T. Tanaka and S. Kato, Numerical simulation of air flow and gas diffusion in a room model. The Fourth International Symposium on the Use of Computers for Environmental Engineering Related to Buildings, 90–95 (1983).
23. P. V. Nielsen, Contaminant distribution in industrial areas with forced ventilation and two-dimensional flow. IIR-Joint Meeting, Commission E1, Essen, F.R.G. (1981).

APPENDIX

The influence of the size and form of the control volume on the calculated U_P is investigated in this appendix. It is assumed below that the velocity field remains the same even if the size of the control volumes is changed.

Consider a control volume (Fig. A1) in a grid in which the distances between the grid lines in the x- and y-direction are δx and δy, respectively. Assume, for simplicity, that the flow (convective as well as diffusive) is directed in the x-direction, $U > 0$, and that the density, ρ, and the diffusion coefficient, Γ, are constant and equal to 1. A source of contaminant, $\dot{m}$, is introduced in this control volume [$\dot{m}$ is kept constant so that U_P = const./c_P, see Eq. (5)]. The discretized equation for this control volume, using hybrid upwind/central differencing, will then be [10]

$$a_P c_P = a_E c_E + a_W c_W + \dot{m} \tag{A1}$$

where,

$$\begin{aligned} a_E &= \max\{0,\ D_e - 0.5F_e\} = \max\{0,\ \delta x\,\delta y - 0.5U_e\delta y\} \\ a_W &= \max\{0,\ D_w - 0.5F_w\} + F_w \\ &= \max\{0,\ \delta x\,\delta y - 0.5U_w\delta y\} + U_w\delta y \\ a_P &= a_W + a_E. \end{aligned} \tag{A2}$$

The D's and F's denote the diffusion and convection, respectively, through the control volume: subscripts e and w refer to east and west face of the control volume, respectively (Fig. A1). From Eqs (A1) and (A2) one expression on c_P when diffusion is dominant (c_P^D) and one expression when convection (c_P^E) is dominant and can be obtained, so that

$$c_P^D = (c_W + c_E)/2 + (\dot{m}\delta y/\delta x)/2 \tag{A3}$$

$$c_P^E = (U_w c_W + \dot{m}/\delta y)/U_w. \tag{A4}$$

From Eq. (A3) it is seen that the second term on the RHS is independent of the configuration of the control volume if $\delta x = \delta y = \delta$. The first term, however, will increase as W and E come closer to P (δ decreases). In order to estimate the dependence of δ on c_P^D, the equation for radial diffusion from a source was solved, i.e.

$$\frac{1}{r}\frac{\partial}{\partial r}\left(\Gamma r\frac{\partial c}{\partial r}\right) = 0 \tag{A5}$$

with a source, $\dot{m}$, introduced in the control volume P at $r = 0$. The boundary condition at the outer boundary was $c = 0$ when $r \to \infty$. Constant Γ was used. Eq. (A5) was solved using finite difference methods. It was found that when δ (which is equal to the radius of the control volume P) was increased by a factor of

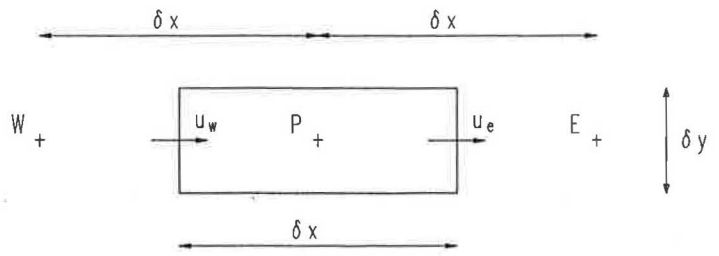

Fig. A1. Control volume P.

2, c_P^D decreased by 14%. c_P^D is thus not very sensitive to variations in δ.

From Eq. (A4) it is gathered that the first term on the RHS is independent of δx and δy, whereas the second term varies inversely with δy. In regions where the convection is much larger than the diffusion the ratio c_W/c_e (subscript 'e' here refers to exit) will be close to 1 (which is confirmed in the calculations); it should be mentioned that this is not the case at the inlet or the outlet where this ratio is close to zero. Replacing of c_e by c_W in Eq. (5) gives

$$\dot{m} = Qc_W. \tag{A6}$$

The two terms on the RHS of Eq. (A4) can, after division by $\dot{m}$ and by use of Eq. (A6), be written

$$1\ Q + 1/(\delta y U_u). \tag{A7}$$

If δy is of the same order as h the two terms in Eq. (A7) are of the same order. It may thus be concluded that c_P^E is inversely dependent on δy if $\delta y \ll h$ and that c_P^E is independent of δy if $\delta y \gg h$.

It has been shown in this appendix that in order to minimize the dependence of the size and the form of the control volumes on the calculated U_P, the sides of the control volumes should be of equal length, δ. The dependence of U_P on δ is then expected to be rather small where diffusion is the dominant transport process. The calculated U_P is more dependent on δ where convection is dominant, if δ is of the same order as (or smaller than) the height of the inlet.

It should be mentioned that the dependence of U_P on δ is not physically incorrect. Since U_P has the physical meaning of (local purging) flow rate (in [kg/s] or [m^3/s]), U_P is expected to be larger the larger the control volume (vessel or compartment) is. It is, however, desirable to minimize this dependence in order to be able to compare calculated U_P in different regions and rooms.